Hindawi
Advances in Civil Engineering
Volume 2019, Article ID 9849635, 14 pages
https://doi.org/10.1155/2019/9849635

Research Article

Similar Material Simulation Study on Protection Effect of Steeply Inclined Upper Protective Layer Mining with Varying Interlayer Distances

Zhigang Yuan,[1,2,3] **Yaohua Shao**,[1] **and Zhuohui Zhu**[1,2,3]

[1]*School of Resources, Environment and Safety Engineering, Hunan University of Science and Technology, Xiangtan, Hunan 411201, China*
[2]*Work Safety Key Lab on Prevention and Control of Gas and Roof Disasters for Southern Coal Mines, Hunan University of Science and Technology, Xiangtan, Hunan 411201, China*
[3]*Hunan Provincial Key Laboratory of Safe Mining Techniques of Coal Mines, Hunan University of Science and Technology, Xiangtan, Hunan 411201, China*

Correspondence should be addressed to Zhigang Yuan; cquyzg@163.com

Received 11 July 2018; Revised 7 December 2018; Accepted 13 January 2019; Published 7 February 2019

Guest Editor: Guang Xu

Protective layer mining, as a dominating regional prevention measure, is generally adopted to prevent and control gas disasters in highly gassy or outburst mines of China. Interlayer distance is one of the most important factors that influences protection effect. However, how does interlayer distance affect the protection effect of steeply inclined upper protective layer mining is not understood fully. According to the engineering practice in Nantong mining district, a new method for similar material simulation experiment of steeply inclined upper protective layer mining is proposed, in which an orthogonal test of similar materials comprising of sand, cement (containing gypsum and fly ash), and water mixture is conducted to obtain relations between proportioning parameters and mechanical properties using a multiple regression method. And then the method is applied to study the protection effect of steeply inclined upper protective layer mining with varying interlayer distances. The results show the following. (1) The proportioning parameters of similar material have strong linear relations with its mechanical properties, and mechanical behaviors of such similar material denote that it can simulate most coal-rock lithologies in coal mine. (2) Both pressure-relief curves and swelling strain curves for protected layer present convex shapes; protection angles at lower excavation boundary are greater than those of upper excavation boundary; with the increase of interlayer distance, the pressure-relief curve evolves from pattern "∩" to pattern "∧" and corresponding pressure-relief region becomes narrower, the center of pressure-relief region tends to transfer to the corresponding center of upper protective layer excavation region, the stress concentration coefficient decreases, the protection angles change little, and the length of the protection region reduces dramatically. (3) The protection region and protection angle calculated based on swelling strain of 3‰ are less than the empirical values based on the dip angle in Provisions, denoting that the method proposed in this study is safer than that in Provisions. The research results provide a useful guide for layouts of roadway and gas drainage boreholes to prevent gas disaster in Nantong coal mine district.

1. Introduction

Currently, coal constitutes a major part of China's energy consumption. As the depletion of shallow coal resources, coal working face would enter into deep mining area. Related studies show that the mining depth of China would increase to 1500 m in next twenty years [1–3]. The in situ stress, gas pressure, or gas content reserved in coal seams would increase with mining depth, thus causing an increase of gas disaster risk which would seriously affect efficiency and safe mining of coal resources. There are numerous measures proposed to prevent and control gas disaster, such as hydraulic fracturing and protective layer mining. Particularly the latter, it has been identified as the dominating regional prevention measure to eliminate gas outburst risk in mining highly gassy mines of China [4, 5]. As illustrated in Figure 1, when there are several

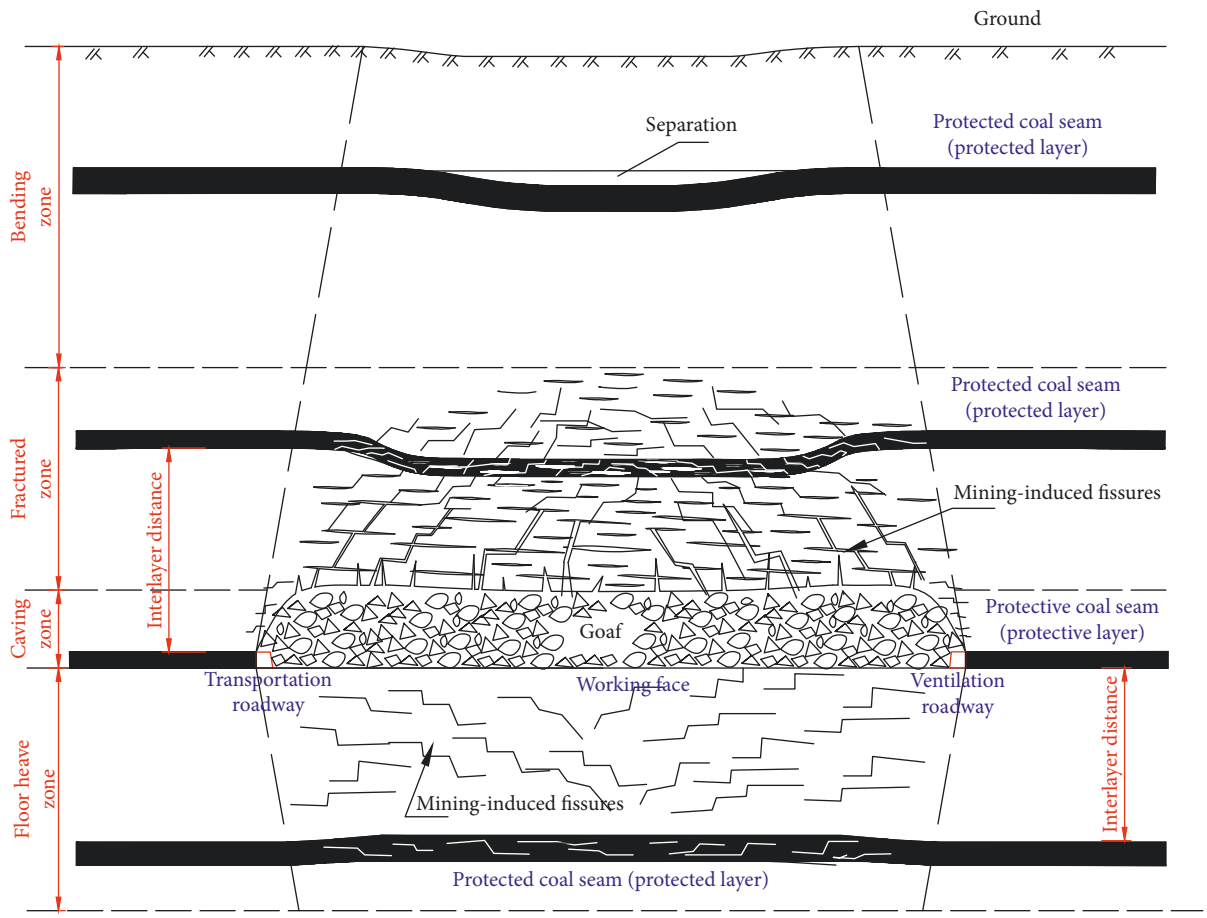

Figure 1: Schematic diagram for protective layer mining.

coal seams (i.e., coal seams group) with gas outburst dangers in highly gassy mine, the coal seam firstly excavated is called protective coal seam or protective layer (the latter is more general as sometimes a thin rock layer is excavated instead in coal mine), while other coal seams excavated later are called protected coal seams or protected layers; the vertical distance between two layers is called interlayer distance. After protective layer is excavated, the stress of surrounding strata would be redistributed, the overlying or underlying strata would move, form fissures, and bed separations as shown in Figure 1. The overlying strata could be subdivided into a caving zone, a fractured zone, and a bending zone from bottom to top, while underlying stratum adjacent to protective layer is a floor heave zone [4, 6]. Because the stresses of adjacent protected layers in specific regions of a caving zone, a fracture zone, and a floor heave zone have been released to an extent, the permeability of protected layers would be increased, causing the coalbed gas to be released continuously through mining-induced fissures or gas drainage boreholes, and gas outburst dangers would be eliminated.

As seen in Figure 1, the protection effects of these protected layers would differ. In the present study, the term "protection effect," which is used to represent comprehensive indexes of the protection angle, protection region, pressure-relief region, swelling strain, and pressure-relief extent, is useful for layouts of transportation/ventilation roadway and gas drainage boreholes in the protected layer, etc. Hence, the determination of protection effect in the protected layer is the key for protective layer mining. There are many factors, such as dip angle and buried depth of coal seam, physicomechanical properties of rock, and interlayer distance, which combine to influence protection effect of protective layer mining. Among these factors, the interlayer distance between two coal seams is a key influencing factor.

Recently, based on theoretical analysis, numerical simulation, and field observation, scholars [7–15] qualitatively studied protection effect of protective layer mining. According to stress distributions of underlying strata and plasticity theory, Yin et al. [10] analyzed the stress-relief principle of underlying strata in theory, and research results showed that, with the increase of mining-induced fissures' depth, underlying strata experienced a less relief of stress whose distribution evolved from pattern "U" to pattern "V," and the protection region became narrower. Li et al. [11] used UDEC program to investigate the pressure-relief effect in near-horizontal protective layer mining with varying interlayer distances. Yang [12] studied stress distribution characteristics of underlying horizontal strata in upper protective layer mining with FLAC^{3D} program, found that underlying strata of protective layer could be divided into a three-dimensional pressure-relief zone, a one-dimensional

pressure-relief zone, and an original stress zone, and then proposed a method based on the stress criterion for classifying close and remote distance protective layer. Based on the assumption that a plastic shear plane exist, Lei et al. [13] obtained an effective interlayer distance for upper protective layer mining using the finite element shear strength reduction method. Wang [14] analyzed the pressure-relief functional principle for underlying strata of the upper protective layer using the numerical method and found that the effective pressure-relief region or swell deformation of underlying strata would gradually reduce with layers space increasing. Liu et al. [15] summarized engineering practices of protective layer mining, proposed an index, "equivalent interval," as the classification criterion of protective layer mining, and suggested that protective layers could be classified as a close distance layer, a remote distance layer, and a super-remote layer. The empirical values for maximum effective interlayer distance and protection angles have been given in "*Provisions of the prevention of coal and gas outburst*" (referred to hereafter as Provisions) [16], but relation between interlayer distance and protection effect has not been proposed.

In brief, existing reports on protection effect of protective layer mining with varying interlayer distances mostly concentrated on slightly inclined or near-horizontal coal seams, lacking reports on steeply inclined coal seams, whose redistribution characteristics of stress and displacement would differ, thus affecting its protection effect [9, 17, 18]; or reports were partially limited to single parameter analysis of protection effect (such as protection angle or pressure-relief region), which could not comprehensively reflect protection effect of protective layer mining; moreover, numerical simulation methods were commonly utilized to investigate rock responses in protective layer mining. The numerical simulation model can be established in computers to study practical engineering, such as anisotropic and discontinuity characteristics of rocks. However, constitutive relations currently used in numerical models have not realistically simulated mechanisms of rock failure or deformation in mesoscopic scale yet [19]. Furthermore, site observations of protection layer mining can be approximated to its realistic conditions. Nevertheless, the engineering geological condition is complex; thus it is difficult to ensure results observed are only affected by single factor (such as interlayer distance) rather than other factors. In short, protection effect of steeply inclined upper protective layer mining with varying interlayer distances is not fully understood and needs further investigation. Compared to site observation and numerical simulation, similar material simulation [20–24] in a laboratory can simulate real physical object (i.e., engineering prototype), with similar materials having mechanical properties similar to those of a prototype according to certain similarity criteria. As the similar material model has all or most of the major characteristics of the prototype, it can reflect failure or deformation process of prototype truly and visually. Moreover, the simulation conditions and variables can be controlled easily, thus a quantitative rule can be observed for research objects with economic feasibility. Hence, according to an engineering practice in Nantong coal mine district, a new method for similar material simulation experiment, with similar materials representing various coal-rock strata around protective layer in coal mine, is conducted to investigate the protection effect of steeply inclined upper protective layer mining with close distance (interlayer distance is 25 m), remote distance (interlayer distance is 45 m), and super-remote distance (interlayer distance is 65 m), respectively [12, 14–16]. The research results provide a useful guide for gas disaster control in Nantong coal mine district. In the sections below, case study mine is introduced in Section 2; the new method for similar material simulation experiment of steeply inclined upper protective layer mining is proposed in Section 3; the protection effect with varying interlayer distances based on similar material experiment is investigated in Section 4; and conclusions are given in the final section.

2. Case Study Mine

The Nantong coal mine district is located in Chongqing city of China, and its geographical location is shown in Figure 2. The coal seams of Nantong coal mine district belong to upper permian longtan formation. The major minable coal seams in this district are C6 coal seam and C4 coal seam.

The schematic diagram for geological synthesis columnar is shown in Figure 3. As seen from Figure 3, the interlayer distance between C6 coal seam and C4 coal seam ranges from 25 m to 70 m due to geologic tectonics. The thickness of C6 coal seam is 1.2~1.8 m with average thickness being 1.5 m, and the thickness of C4 coal seam is 1.8~2.2 m with average thickness being 2 m. The average dip angle for two coal seams is 45°, which are steeply inclined coal seams. The strata lithologies between two coal seams are mainly calcareous shale, silty shale, limestone, and cherty limestone.

Currently, the average buried depth of C6 coal seam, overlying above the C4 coal seam, is 650 m. The C6 coal seam has lower risk of gas outburst, so it is chosen as the upper protective layer to eliminate gas outburst risk of C4 coal seam. A pitching oblique mining method [9, 17] is used to exploit coal seams, and the average working face length in C6 coal seam is 70 m. Related physicomechanical parameters for each stratum are shown in Table 1.

As mentioned, the dip angle and buried depth of C6 coal seams do not vary largely, but the interlayer distance between two mineable coal seams ranges from 25 m to 70 m. To systematically and accurately study protection effect of steeply inclined upper protective layer mining with varying interlayer distances, the interlayer distances chosen to be studied should reflect conditions of close distance, remote distance, and super-remote distance. There are no acknowledged definitions of close distance, remote distance, and super-remote distance protective layers presently. But relevant studies [12, 14–16] showed that, with the increase of interlayer distance, the pressure-relief effect in the protected layer would decrease; when it reaches to an extent, the protection effect cannot be guaranteed. The Provisions [16] points out that the maximum effective interlayer distance for steeply inclined upper protective layer mining is 60 m. Liu et al. [15] proposed an index, "equivalent interval," as the classification criterion of protective layers. The equivalent interval is defined as (interlayer distance)/(mining height).

Figure 2: Location map of Nantong coal mine district.

When the equivalent interval is less than 20, it is called the close distance protective layer. When the equivalent interval is greater than 20 but less than 50, it is called the remote distance protective layer. Yang [12] proposed a method based on the stress criterion for classifying close and remote distance protective layer. Results showed that when the mining height is 1.5 m, when the interlayer distance is less than 30 m, it is called the close distance protective layer; when the interlayer distance is greater than 30 m but less than 64 m, it is called the remote distance protective layer. Therefore, based on the geological synthesis columnar of Nantong coal mine district and aforementioned studies, close distance (interlayer distance is 25 m), remote distance (interlayer distance is 45 m), and super-remote distance (interlayer distance is 65 m) are chosen in this paper to investigate the influence of varying interlayer distances on protection effect of steeply inclined upper protective layer mining, which can well reflect the actual situation of Nantong coal mine district.

3. Similar Material Simulation Experiment

3.1. Experimental Devices. In order to carry out the similar material simulation experiment, a rotatable physical similarity simulation bench, with the geometric dimensions of 2.0 m × 2.0 m × 0.3 m (length × height × width) and rotation angles ranging from 0° to 70° to manufacture coal-rock strata with various dip angles, is used, and other experimental devices consisting of pressure test devices, strain (or displacement) test devices, and loading devices (including levers and weights) are shown in Figure 4. It is worth noting that, after the similar material simulation model has been manufactured, the ground pressure induced by excluded overlying strata is applied using levers, of which the ratio of power arm to resisting arm is 1 : 10, on the top of the similar material model as shown in Figure 4.

3.2. Similarity Condition and Similar Material

3.2.1. Parameter Determination of Interlayer Lithology. As seen from Figure 3 and Table 1, there are various kinds of strata with different physicomechanical properties and thicknesses between upper protective layer (C6 coal seam) and protected layer (C4 coal seam). The variation of interlayer distance inevitably results in thickness change of each stratum, thus causing the difficulty of studying effect of interlayer distance on protection effect of steeply inclined upper protective layer mining. Relevant studies [14, 18] showed that the "thickness weighted average method" (referred to hereafter as TWAM), which combines several strata into a composite medium stratum or introduces interbedded hard rock content coefficient, can reflect integrated physicomechanical behavior of coal-rock strata between two coal seams. Therefore, TWAM is utilized to eliminate the influence of interlayer lithology:

$$X = \frac{\sum_{i=1}^{n} l_i X_i}{\sum_{i=1}^{n} l_i}, \tag{1}$$

where X denotes weighted average of the physicomechanical parameter for composite medium stratum between two coal

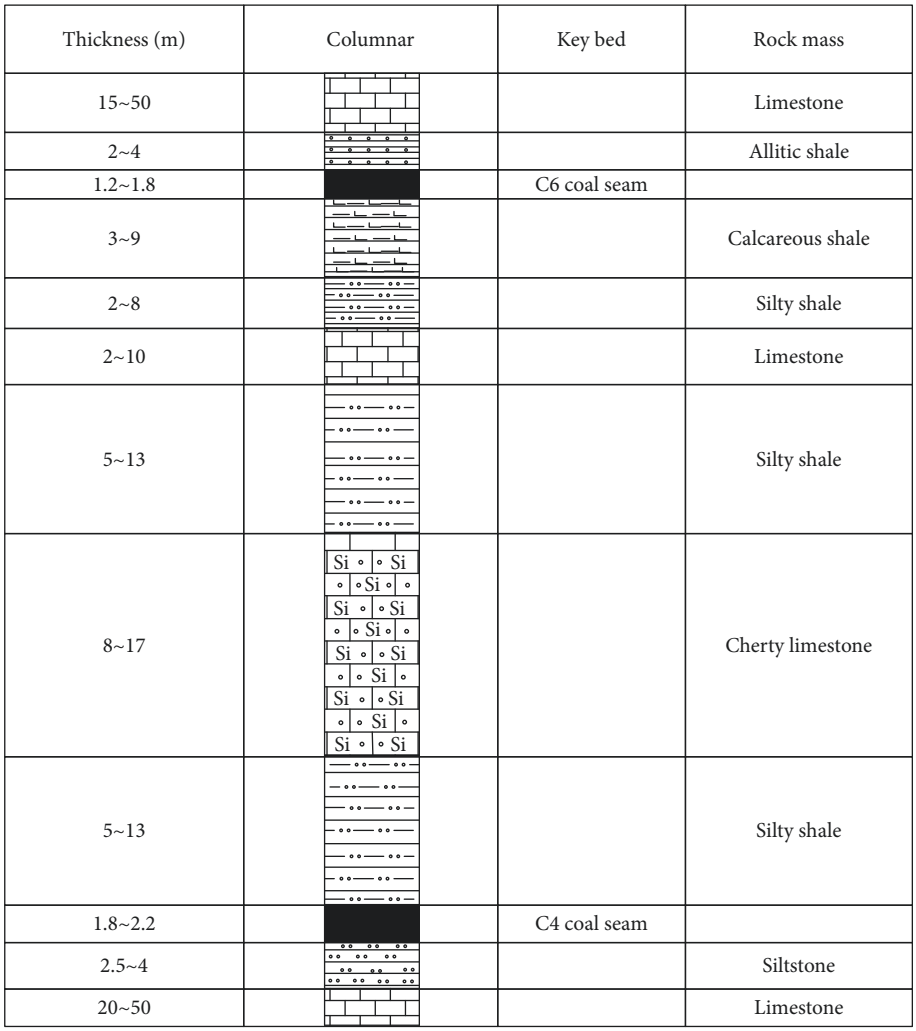

Figure 3: Schematic diagram for geological synthesis columnar.

Table 1: Related physicomechanical parameters for each stratum.

Stratum number	Lithology	Volume weight ($MN \cdot m^{-3}$)	Elastic modulus (GPa)	Poisson's ratio	Tensile strength (MPa)	Compressive strength (MPa)
1	Limestone	0.028	30.2	0.26	9.8	107.35
2	Allitic shale	0.024	23.3	0.30	6.6	91.00
3	C6 coal seam	0.014	0.91	0.35	0.4	3.98
4	Calcareous shale	0.025	26.4	0.23	8.7	103.35
5	Silty shale	0.024	23.1	0.28	9.8	107.35
6	Limestone	0.028	30.2	0.26	9.8	107.35
7	Silty shale	0.024	27.6	0.28	6.6	88.71
8	Cherty limestone	0.029	35.3	0.23	21.2	185.26
9	Silty shale	0.024	20.1	0.28	9.8	107.35
10	C4 coal seam	0.014	0.94	0.38	0.3	3.38
11	Siltstone	0.030	21.6	0.25	7.3	104.57
12	Limestone	0.028	30.2	0.26	9.8	107.35

seams, X_i denotes physicomechanical parameter for ith stratum, l_i denotes the ith stratum thickness, and n denotes the number of strata.

3.2.2. Similarity Criteria and Similar Material. The similar material simulation experiment is a reduced-scale approach according to similarity criteria [24–26]. The selected similar

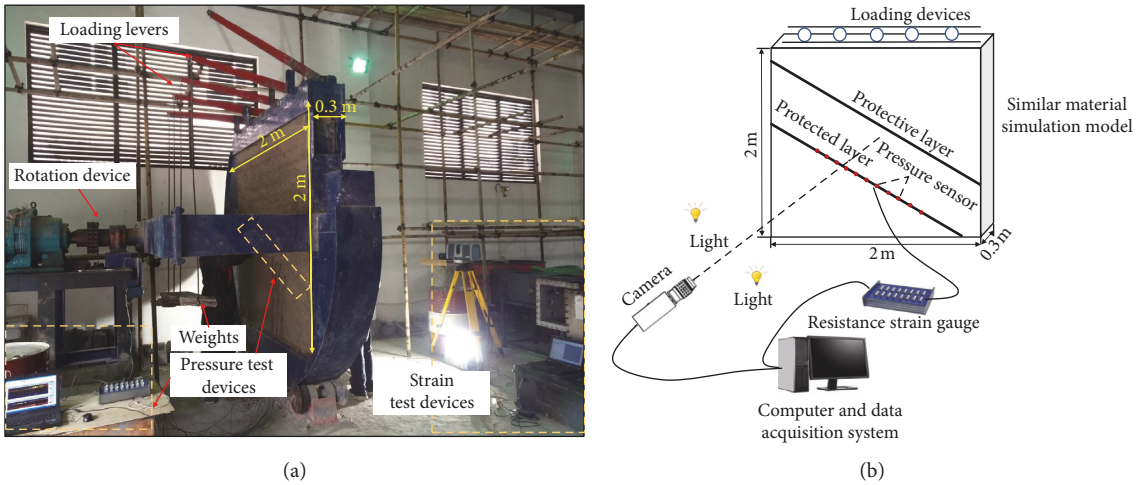

Figure 4: Experimental devices (a) and setup (b) for similar material simulation.

materials must have very similar physicomechanical properties of engineering prototype (referred as coal-rock strata here). At present, similarity criteria are based on elastic theory and dimensional analysis method. According to the pressure-relief mechanism of protective layer mining, the following similarity criteria should be satisfied in similar material simulation experiment [22–24]:

$$(\sigma_t)_m = \frac{L_m}{L_p} \times \frac{\gamma_m}{\gamma_p} \times (\sigma_t)_p, \tag{2}$$

$$(\sigma_c)_m = \frac{L_m}{L_p} \times \frac{\gamma_m}{\gamma_p} \times (\sigma_c)_p, \tag{3}$$

$$C_m = \frac{L_m}{L_p} \times \frac{\gamma_m}{\gamma_p} \times C_p, \tag{4}$$

$$\tan(\varphi_m) = \tan(\varphi_p), \tag{5}$$

$$E_m = \frac{L_m}{L_p} \times \frac{\gamma_m}{\gamma_p} \times E_p, \tag{6}$$

$$\nu_m = \nu_p, \tag{7}$$

where $(\sigma_t)_p$, L_p, γ_p, $(\sigma_c)_p$, C_p, φ_p, E_p, and ν_p denote the tensile strength, geometric size, volume weight, compressive strength, cohesion, internal friction angle, elastic modulus, and Poisson's ratio of coal-rock prototype, respectively; $(\sigma_t)_m$, L_m, γ_m, $(\sigma_c)_m$, C_m, φ_m, E_m, and ν_m denote the tensile strength, geometric size, volume weight, compressive strength, cohesion, internal friction angle, elastic modulus, and Poisson's ratio of similar material, respectively. Taking into account geometric size of laboratory physical similarity simulation bench, the geometric similarity constant L_m/L_p is set to 1/100, and scales of other physicomechanical parameters can be derived from equations (2)–(7).

To implement similar material simulation experiment, a suitable similar material is needed. The type and proportion parameters of similar material determine whether experimental results obtained can represent mechanical responses of prototype. Similar material simulation experiments have been widely employed, but how to obtain accurate and optimum proportioning parameters is urgently needed to be investigated in coal mining [20–26]. In this section, the river sand, cement (containing gypsum and fly ash), and water are used and mixed to manufacture a new similar material, which is used to represent various coal-rock strata around the protective layer in the coal mine. The composition ratios of similar material, such as sand-binder ratio (i.e., river sand to cement ratio), density, and residual water content, have significant influence on its mechanical responses. To obtain accurate proportioning parameters, based on the orthogonal design method and multiple regression method, relations between mechanical parameters and proportioning parameters of such similar material are obtained, and then the required mixing ratio and manufacture parameters for similar material simulation experiment can be accurately deduced.

The three influencing factors (including sand-binder ratio, density and residual water content) are relaxed within specific regions, and each factor is divided into four levels; then Poisson's ratio, compressive strength, and elastic modulus are determined. The orthogonal array $L_{16}(4^3)$ is applied to choose sixteen combinations to be tested [21–23]. The levels of orthogonal design for similar materials are shown in Table 2, and the sixteen combinations and corresponding mechanical parameters obtained are given in Table 3.

It is worth noting that mechanical parameters (including Poisson's ratio, compressive strength, and elastic modulus) are obtained by uniaxial compression tests of similar material specimens with a diameter and a height of 50 mm and 100 mm in the laboratory, as shown in Figure 5.

As can be seen from Table 3, the elastic modulus, compressive strength, and Poisson's ratio of similar material specimens range from 27.36~261.84 MPa, 0.181~1.202 MPa, and 0.149~0.343, respectively. The testing results denote that mechanical behaviors of similar material have a large variation range, which can satisfy requirements of similar

Table 2: Levels of orthogonal design for similar materials.

Level number	Sand-binder ratio	Density (kg·m^{-3})	Water content (%)
1	6	1550	5
2	8	1600	3
3	10	1650	2
4	12	1700	1

Table 3: Sixteen combinations and mechanical parameters of similar materials.

Experimental number	Sand-binder ratio	Density (kg·m^{-3})	Residual water content (%)	Compressive strength (MPa)	Elastic modulus (MPa)	Poisson's ratio
1	6	1550	5	0.442	91.23	0.251
2	6	1600	3	0.504	81.67	0.254
3	6	1650	2	0.821	217.83	0.213
4	6	1700	1	1.202	261.84	0.243
5	8	1550	3	0.270	48.75	0.235
6	8	1600	5	0.416	74.36	0.296
7	8	1650	1	0.572	96.42	0.194
8	8	1700	2	0.731	166.22	0.284
9	10	1550	2	0.315	59.22	0.190
10	10	1600	1	0.333	65.51	0.186
11	10	1650	5	0.181	27.36	0.311
12	10	1700	3	0.354	53.88	0.316
13	12	1550	1	0.193	47.02	0.149
14	12	1600	2	0.206	38.50	0.202
15	12	1650	3	0.239	40.60	0.286
16	12	1700	5	0.267	43.84	0.343

Figure 5: Mechanical testing of similar material specimens.

material simulation experiment with various coal-rock lithologies in the present study.

Utilizing the multiple regression method [27], the regression equations between proportioning parameters and mechanical parameters are obtained according to testing results in Table 3:

$$S = 0.00218x - 0.0657y - 0.0875z - 2.13, \quad (8)$$

$$E = 0.48x - 17.03y - 20.3z - 462, \quad (9)$$

$$\nu = 0.000574x + 0.0273y - 0.762, \quad (10)$$

where S, E, ν, x, y, and z denote compressive strength, elastic modulus, Poisson's ratio, density, residual water content, and sand-binder ratio, respectively. The fitting correlation coefficients for equations (8)–(10) are 0.87, 0.9, and 0.93, which indicate that strong linear relations exist between mechanical parameters and proportioning parameters.

According to equations (8)–(10), the effects of sand-binder ratio on compressive strength and elastic modulus are more remarkable than the effects of the residual water content and density; both compressive strength and elastic modulus of similar materials increase as the density increases and decrease as the residual water content or sand-binder ratio increases; the effect of residual water content on Poisson's ratio is more remarkable than the effect of density, and sand-binder ratio has little effect on Poisson's ratio of similar materials.

Finally, proportioning parameters for each coal-rock stratum in the similar material simulation experiment can be derived by solving equations (8)–(10) using the Matlab program:

$$x = 5640.8\nu - 19306S + 83.235E - 1493.7, \quad (11)$$

$$y = 4.06S - 0.782\nu - 0.175E + 1.1091, \quad (12)$$

$$z = 3.387E + 194.71\nu - 797.03S - 15.492. \quad (13)$$

According to the physicomechanical properties of each stratum in Table 1, geometric similarity constant, and equations (11)–(13), the final proportioning ratios and physicomechanical parameters for similar material representing each stratum are obtained, as shown in Table 4.

3.3. Model Manufacture and Experimental Procedure

3.3.1. Model Manufacture. The coal-rock strata of on-site engineering are simulated by similar materials including sand, cement (containing gypsum and fly ash), and water mixtures. To ensure proportioning ratios and mechanical parameters for each stratum are satisfied, similar material for each stratum or layer is manufactured using a method of layered filling and compaction [24], in which a moderate amount of mica powder is sprinkled between different layers as laminated weak surfaces. The physical similarity simulation bench should be firstly rotated an angle of 45° to perform the filling of similar materials. The thickness of each stratum and excavation length in similar material simulation model are determined according to geometric similarity constant of 1 : 100. The complete similar material model including each rock formation is illustrated in Figure 6. For better clarity, the relevant rock strata in the similar material model have been marked. To reduce boundary effect of upper protective layer mining [17, 18], the simulated working face of C6 coal seam (i.e., protective layer) is arranged at the approximate diagonal of the similar material simulation model.

The main purposes of this experiment are to study pressure-relief characteristics and deformations within underlying C4 coal seam (protected layer) induced by C6 coal seam (protective layer) mining. Hence, internal pressures and deformations (or strains) within the protected layer are needed to be monitored during excavation. The internal pressures are monitored using ASMD3-16 resistance strain gauge and BX-1 pressure sensors, while the displacements (or strains) are monitored using a digital image correlation method [24], as shown in Figure 7.

The locations in the C4 protected layer, which correspond to upper and lower boundaries of the C6 protective layer excavation region, generally have minimum swelling deformation. Thus, the variations of pressure and displacement nearby these positions are keys for determining protection angle and protection region. Taking such into account, pressure sensors with an interval are embedded in the C4 protected layer to record the pressures, whose embedding locations correspond to the excavation region of the C6 protective layer. In addition, as image coordinates and similar material model coordinates need to be corresponded when the digital image correlation method is used to compute displacement and strain after the C6 protective layer excavation, some grid points (i.e., control reference points) are also arranged on similar model surface [24] as shown in Figure 6. Similar material simulation results given below indicate that the method used can achieve a comprehensive monitoring of displacement and pressure during C6 protective layer mining. Furthermore, the average buried depth of the C6 protective layer in the similar material model is 800 mm, which represents 80 m in the prototype. To simulate C6 protective layer mining in Nantong coal mine district with an average buried depth of 650 m, the ground pressure induced by excluded overlying strata with an average thickness of about 570 m is applied as an additional uniform load using levers on the top of the similar material model. According to the aforementioned similarity criteria for similar material model and lever principle, fifty-seven weights, whose mass of each is 10 kg, are applied on five levers to simulate the ground pressure as shown in Figure 4(a).

3.3.2. Experimental Procedure. The data acquisition system of pressure and displacement should be calibrated and reset before excavation. When the maintenance time of similar material model reaches (20–30 days in general), and the similar material strength satisfies the designed requirements, the C6 coal seam is excavated with a length of 700 mm to simulate C6 coal seam mining, which can be shown in Figure 6. During the excavation of C6 coal seam, the pressure data measured by pressure sensors are monitored and collected, and the procedure for collecting deformation and strain of protected layer is as follows: (1) photos of the similar material model are taken by a high-precision digital camera; (2) the recorded photos are analyzed in order by software GeoDIC; (3) figures for deformation and strain fields of strata are obtained using the result visualization postprocessing system PostViewer. It is worth noting that the monitoring data are collected until the excavation has been completed and the strata deformation is stable.

4. Results and Analysis of Protection Effect with Varying Interlayer Distances

4.1. Pressure-Relief Characteristics of Protected Layers with Varying Interlayer Distances. The schematic diagram for relevant parameters in upper protective layer mining is illustrated in Figure 8. The term "DBMC" represents distance along bedding surface between monitoring point of C4 protected layer and central point of C6 protective layer excavation region. The term "offset distance" represents the bedding distance between the central point of pressure-relief region and the central point of C6 protective layer excavation region. Therefore, if the value of DBMC is positive, it denotes the monitoring point is located at the ascending direction of the C4 protected layer corresponding to excavation region of the C6 protective layer, and vice versa. If the offset distance is zero, it denotes the pressure-relief region is symmetric with central point of the C6 protective layer excavation region.

Table 4: Proportioning parameters and mechanical parameters of similar materials for each stratum.

Stratum number	Lithology	Density (kg·m^{-3})	Sand-binder ratio Sand : cement	Elastic modulus (MPa)	Compressive strength (MPa)
1	Limestone	1.656	6 : 1	178.61	0.63
2	Allitic shale	1.637	6 : 1	162.31	0.63
3	C6 coal seam	1.513	9 : 1	10.19	0.04
4	Composite medium stratum	1.551	6.5 : 1	140.80	0.70
5	C4 coal seam	1.513	9 : 1	10.09	0.04
6	Siltstone	1.539	7 : 1	110.81	0.54
7	Limestone	1.656	6 : 1	178.61	0.63

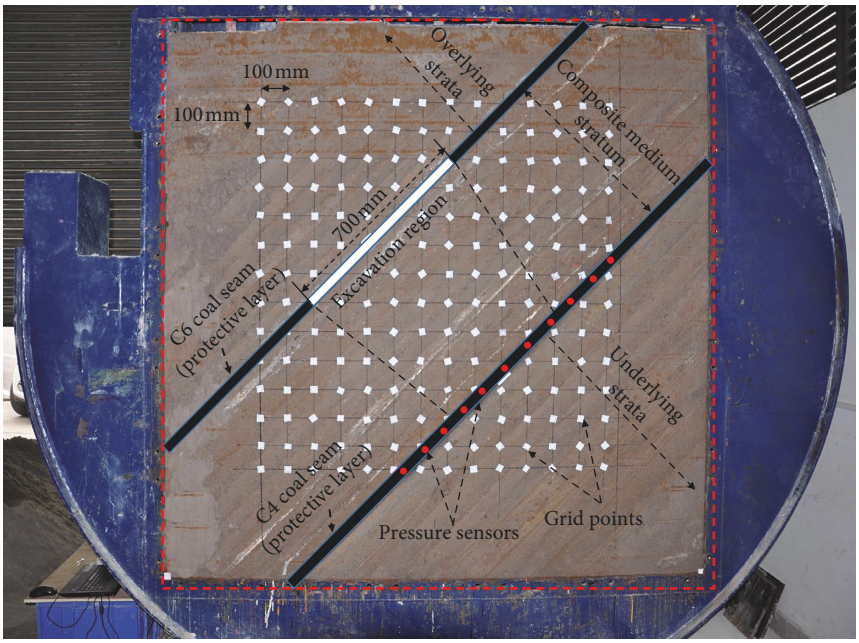

Figure 6: Similar material model.

(a) (b)

Figure 7: Pressure monitoring devices. (a) Pressure sensor. (b) Resistance strain gauge.

After the C6 protective layer has been excavated, pressure-relief curves for C4 protected layers with varying interlayer distances are obtained through analysis of monitoring results of pressure sensors, as shown in Figure 9.

In Figure 9, the vertical coordinate represents the pressure-relief value of ground stress within the C4 protected layer. Therefore, if the pressure-relief value is greater than zero, it denotes that the ground stress within the C4 protected layer would be released; namely, it is less than its initial value, and vice versa. The shapes of pressure-relief curves for C4 protected layers with varying interlayer distances are both convex. The curve slopes are greater on both sides of curve boundaries, indicating that the pressure-relief extents significantly change near boundaries of corresponding excavation regions. With the increase of interlayer distance, the pressure-relief curve evolves from pattern "∩" to pattern "∧" and corresponding pressure-relief region becomes narrower, which agrees with the relevant theoretical analysis results [10]; the altitude of pressure-relief curve decreases, indicating that the overall pressure-relief

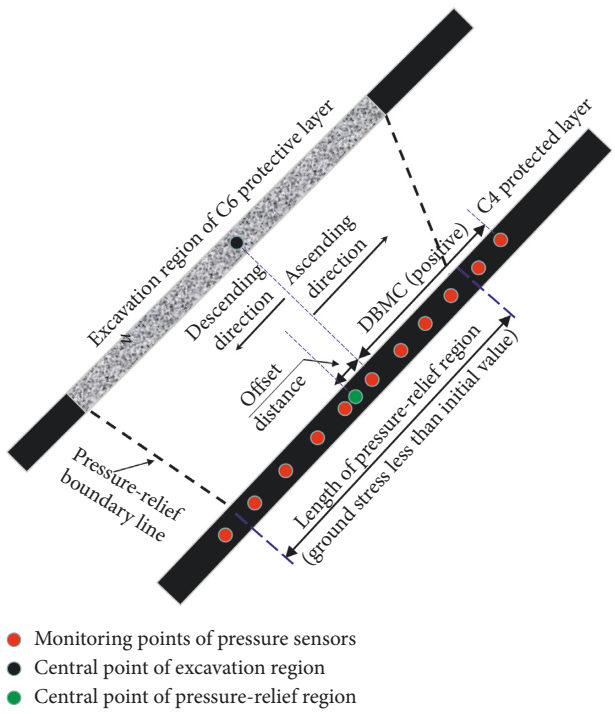

Figure 8: Schematic diagram for relevant parameters in upper protective layer mining.

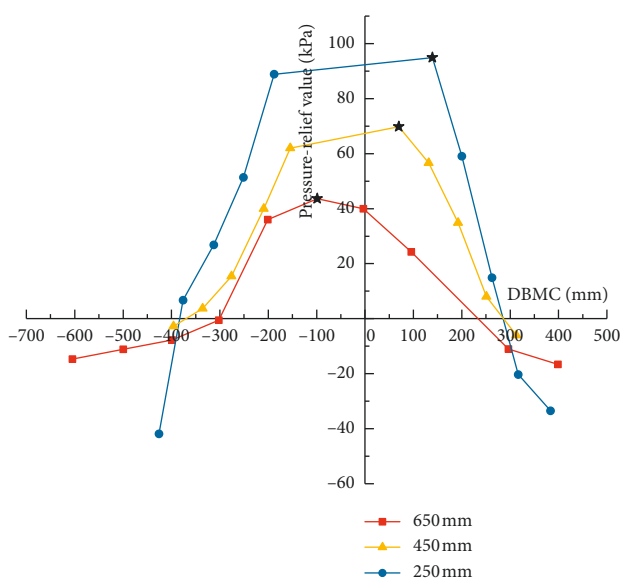

Figure 9: Pressure-relief curves for C4 protected layers with varying interlayer distances.

extent of the protected layer reduces; and curve slopes on both sides of the curve boundaries decrease, indicating that the stress concentration nearby excavation boundaries of protective layer reduces, but the influencing range of pressure concentration increases; furthermore, the drop velocity of the pressure-relief curve in the ascending direction is greater than that of the descending direction, and the maximum pressure-relief point (denoted by "★" in Figure 9) gradually evolves from the ascending direction to descending direction, which are distinctly discrepant with the characteristics of pressure-relief curves in lower protective layer mining [28].

4.1.1. Characteristics of Pressure-Relief Regions. As aforementioned, if the pressure-relief value is greater than zero, it indicates that the ground pressure is less than the initial pressure, thus the distance between the two intersection points of pressure-relief curve and horizontal coordinate is the length of pressure-relief region (Figure 8). The length of pressure-relief region and offset distance with varying interlayer distances are presented in Table 5. As seen in Table 5, with the increase of interlayer distance, the length of pressure-relief region decreases monotonously from 669 mm to 504 mm, while offset distance increases monotonously from −50 mm to −46 mm, indicating that the center of the pressure-relief region tends to transfer to the corresponding center of C6 protective layer excavation region.

4.1.2. Maximum Pressure-Relief Values and Pressure-Relief Ratios. The pressure-relief ratio η_p is given by $\eta_p = |\sigma - \sigma_0|/\sigma_0$, where σ_0 is the original pressure within the protected layer before C6 coal seam excavation and σ is the pressure within protected layer after C6 coal seam excavation. The maximum pressure-relief value and maximum pressure-relief ratio with varying interlayer distances are presented in Table 6. Both the maximum pressure-relief value and pressure-relief ratio decrease as interlayer distance increases, which indicate that effects of C6 protective layer mining on underlying protected layer would be gradually reduced. It can be concluded that the protection effect would be diminished when the interlayer distance increases to an extent, which conforms to the practical situation.

4.1.3. Pressure Concentration Coefficients. The pressure concentration coefficient η_c is given by $\eta_c = \sigma/\sigma_0$. Two locations in C4 protected layers are chosen to analyze the stress concentration coefficient, one is in the descending direction with DBMC being −427.6 mm, and the other is in the ascending direction with DBMC being 377.5 mm. During excavation of the C6 upper protective layer with interlayer distance being 450 mm, no pressure concentration is observed as all pressure sensors are arranged in the pressure-relief region. So only the pressure concentration coefficients with interlayer distances being 250 mm and 650 mm are obtained in Table 7. As seen from Table 7, with interlayer distance increasing, the pressure concentration coefficients at the descending and ascending locations both decrease, indicating that the effects of protective layer mining on underlying protected layers also decrease.

In brief, as the interlayer distance increases, the pressure distribution pattern in the protected layer evolves from "U" to "V"; the pressure concentration coefficient in the protected layer decreases, but the influencing range of pressure concentration increases; the maximum pressure-relief ratio decreases, which are 50.8%, 37%, and 23.5% in the close,

Table 5: Pressure-relief region and offset distance with varying interlayer distances.

Interlayer distance (mm)	Length of pressure-relief region (mm)	Offset distance (mm)
250	669	−50
450	652	−47
650	504	−46

Table 6: Maximum pressure-relief value and pressure-relief ratio with varying interlayer distances.

Interlayer distance (mm)	Maximum pressure-relief value (kPa)	Maximum pressure-relief ratio (%)
250	94.80	50.8
450	68.99	37
650	43.89	23.5

Table 7: Pressure concentration coefficient with varying interlayer distances.

Interlayer distance (mm)	Pressure concentration coefficient at descending location	Pressure concentration coefficient at ascending location
250	1.218	1.202
650	1.046	1.080

remote, and super-remote distance protected layers, respectively; and the length of pressure-relief region decreases, which are 669 mm, 652 mm, and 504 mm in the close, remote, and super-remote distance protected layers, respectively. According to the above results, a large pressure-relief region will develop in the underlying protected layer and lead to a significant increase in coal permeability in Nantong coal mine district [2, 3]. Therefore, upper protective layer mining combined with gas drainage in pressure-relief region can be adopted to prevent gas outburst and guide layout of roadway in site. As the stresses in the pressure-relief region have been released to an extent, the difficulty degree of gas drainage in the pressure-relief region is greatly reduced compared with other regions. Gas drainage boreholes should be drilled in the pressure-relief region before C6 upper protective layer mining, which is to ensure the pressure-relief gas can be extracted timely. Besides, the middle section or length of pressure-relief region for close distance or remote distance protective layer mining is flatter or greater than that of super-remote distance protective layer mining. Hence, the spacings or of gas drainage boreholes in super-remote distance protective layer mining should be reduced. Moreover, the stress in location with the maximum pressure-relief ratio has been released more fully, and the location of pressure-relief region center tends to transfer to the excavation region center as interlayer distance increases, and thus the two locations are key regions for gas drainage. Furthermore, the influencing range of pressure concentration increases with interlayer distance increasing. Hence, the roadway in super-remote distance protective layer mining should be arranged at a greater distance from the corresponding excavation boundary.

4.2. Protection Regions and Angles with Varying Interlayer Distances. After the excavation of the C6 protective layer, according to the digital image correlation method [24], the displacements in the normal direction of protected layers for the similar material model with varying interlayer distances can be calculated. And then through transformation and calculation, the swelling strains within protected layers can be obtained. The swelling strain curves for protected layers with varying interlayer distances are illustrated in Figure 10. It indicates that the distribution characteristics of swelling strains within C4 protected layers are similar to that of pressures (as shown in Figure 9), which also demonstrates that a strong relation exists between pressure and strain in upper protective layer mining. With the increase of interlayer distance, the swelling strain curve evolves from pattern "∩" to pattern "∧" and corresponding region with positive swelling strain becomes narrower; the altitude of swelling strain curve decreases, indicating that the overall strain of protected layer reduces; and curve slopes on both sides of the curve boundaries decrease.

In current Provisions [16], if the coal-rock lithologies and mining heights change little between protected layer and protective layer, when the swelling strains of specific region within the protected layer are equal or greater than 3‰, the gas outburst risk within such specific region of the protected layer would be eliminated. Such specific region is called the protection region. Hence, swelling strain of 3‰ (referred to hereafter as the deformation protection criterion) is used to ascertain the protection region within the protected layer in the present study. Based on the deformation protection criterion, the protection angle at the lower excavation boundary of the C6 protective layer is given by

$$\delta_3 = \arctan\left(\frac{h}{u}\right), \tag{14}$$

where δ_3 represents the protection angle at the lower excavation boundary of the protective layer, h is the interlayer distance between protected layer and protective layer, and u is the distance along bedding surface between lower excavation boundary of the C6 protective layer and the critical point with swelling strain of 3‰, as shown in Figure 11. The

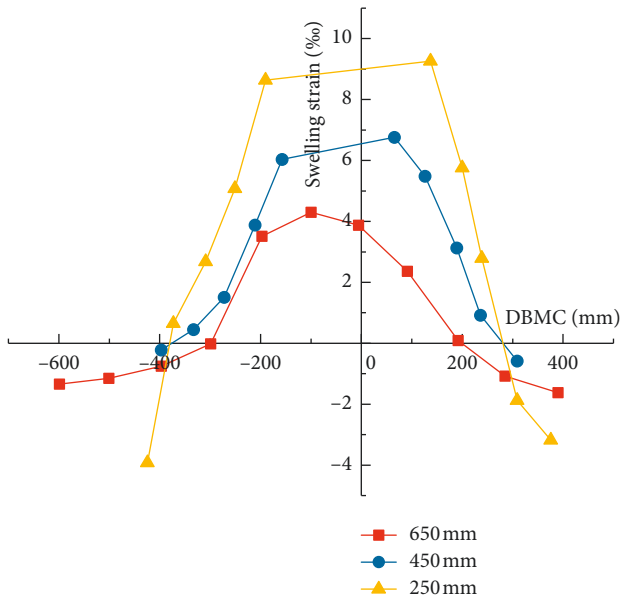

Figure 10: Swelling strain curves for the C4 protected layer with varying interlayer distances.

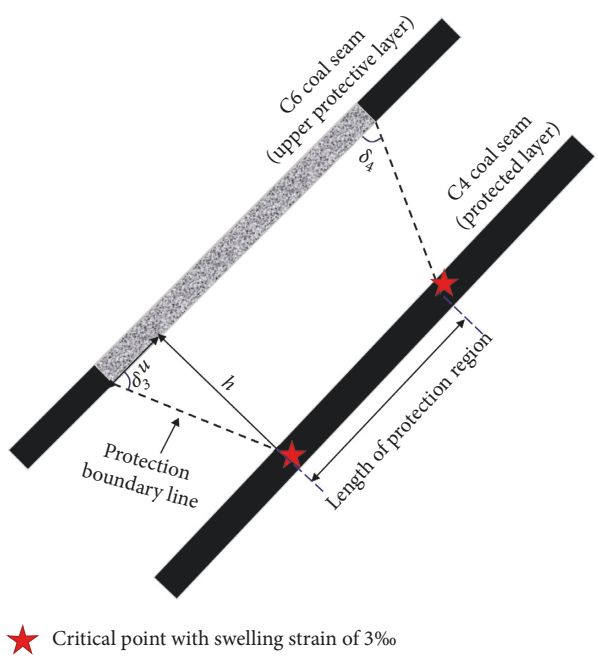

Figure 11: Schematic diagram for calculation of protection angles.

calculation method for the protection angle at the upper excavation boundary of the C6 protective layer, δ_4, is similar to that of the lower excavation boundary.

Protection angles at excavation boundary of C6 protective layers are calculated using equation (14), and the empirical values in Provisions are also given for comparison, as shown in Table 8. As seen from Table 8, protection angles at the lower excavation boundary are greater than that of the upper excavation boundary. As the interlayer distance increases, protection angles at lower and upper excavation boundaries change little. The average protection angles at lower and upper excavation boundaries are 77° and 67°, respectively, both of which are less than the empirical values in Provisions.

Related studies show that the underlying floor be divided into floor heave-induced fissure zone, floor heave-induced deformation zone, and original floor zone from top to bottom [29–31]. In the former zone, mining-induced fissures propagate across or parallel to bedding planes, and thus gas can easily flow to the goaf through fissures. In the second zone, fissures are mainly parallel with bedding planes, thus providing channels for gas migration. In the third zone, there are little fissure channels for pressure-relief gas migration, and thus the protection effect cannot be guaranteed. The lower limit of the floor heave-induced fissure zone is 15~25 m, while the lower limit of the floor heave-induced deformation zone is 50~60 m. Therefore, the close, remote, and super-remote distance protected layers in the present study are in the floor heave-induced fissure zone, the floor heave-induced deformation zone, and the original floor zone, respectively. The protection effect of the super-remote distance protective layer mining cannot be guaranteed. The relation between length of protection region and interlayer distance is presented in Figure 12. As shown in Figure 12, with the increase of interlayer distance, the length of the protection region reduces dramatically. The length of the protection region decreases from 434.5 mm to 268.7 mm for remote and super-remote distance protective layer mining, which agrees well with the aforementioned analysis results. Engineering practice in Nantong coal mine district also verifies that the protection effect of protective layer mining with super-remote distance cannot be guaranteed. Thus, compared with close distance or remote distance protective layer mining, more measures should be taken to enhance gas drainage to eliminate the gas outburst risks of the super-remote distance protected layer in Nantong coal mine district [29].

In brief, when mining steeply inclined upper protective layer with varying interlayer distances in Nantong coal mine district, both the protection region and protection angle determined based on the deformation protection criterion are less than the empirical values based on the dip angle in Provisions, denoting that the method proposed in this study is safer than that in Provisions.

5. Conclusions

According to an engineering practice of Nantong coal mine district, a method for the similar material simulation experiment of steeply inclined upper protective layer mining is proposed, and then it is adopted to investigate the protection effect with varying distances. The obtained conclusions are as follows:

(1) The new similar material, which comprises of sand, cement (containing gypsum and fly ash), and water mixture, can simulate various coal-rock lithologies in coal mine.

(2) Strong linear relations exist between mechanical parameters and proportioning parameters of similar

Table 8: Protection angle at the excavation boundary.

Interlayer distance (mm)	Protection angle at the lower excavation boundary, δ_3 (°)		Protection angle at the upper excavation boundary, δ_4 (°)	
	Present results	Results in Provisions	Present results	Results in Provisions
250	78	80	65	70
450	75	80	71	70
650	78	80	65	70

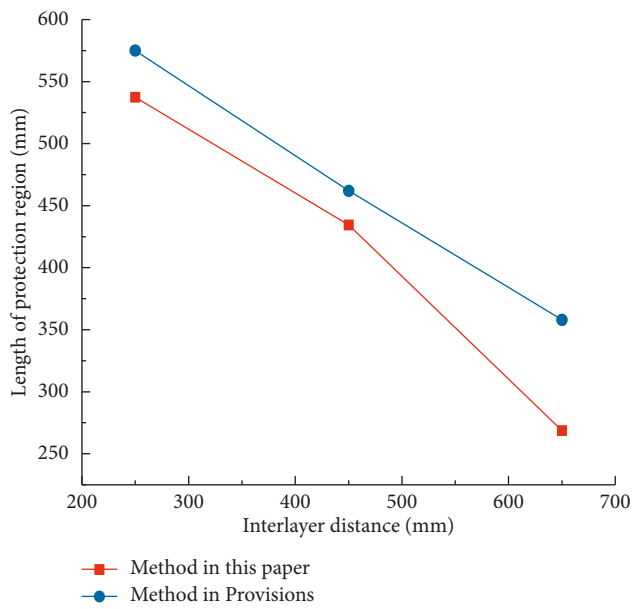

Figure 12: Relationship between length of protection region and interlayer distance.

material. The effects of the sand-binder ratio on compressive strength and elastic modulus are more remarkable than the effect of the density and residual water content; both the compressive strength and elastic modulus of similar materials increase as the density increases and decrease as the residual water content or sand-binder ratio increases; the effect of residual water content on Poisson's ratio is more remarkable than the effect of density, and sand-binder ratio has little effect on Poisson's ratio of similar materials.

(3) Both pressure-relief curves and swelling strain curves for the protected layer present convex shapes. With the increase of interlayer distance, the pressure-relief curve evolves from pattern "∩" to pattern "∧" and corresponding pressure-relief region becomes narrower; the center of pressure-relief region tends to transfer to corresponding center of protective layer excavation region; the maximum pressure-relief value, pressure-relief ratio, and stress concentration coefficient decrease; the protection angles change little, but length of protection region reduces dramatically. Both protection region and protection angle based on swelling strain of 3‰ in the present study are safer than that in Provisions. The research results provide a useful guide for layouts of roadway and gas drainage boreholes to prevent gas disaster in Nantong coal mine district.

Data Availability

The data used to support the findings of this study are included within the article.

Conflicts of Interest

The authors declare that there are no conflicts of interest regarding the publication of this paper.

Acknowledgments

This work was supported by the National Natural Science Foundation of China (Grant no. 51604111); the Scientific Research Fund of Hunan Provincial Education Department (Grant no. 16C0654); and the Doctoral Scientific Research Foundation of Hunan University of Science and Technology (Grant no. E51502).

References

[1] Z. Zhu, T. Feng, Z. Yuan, D. Xie, and W. Chen, "Solid-gas coupling model for coal-rock mass deformation and pressure relief gas flow in protection layer mining," *Advances in Civil Engineering*, vol. 2018, Article ID 5162628, 6 pages, 2018.

[2] Y. P. Cheng, H. Y. Liu, P. K. Guo et al., "A theoretical model and evolution characteristic of mining-enhanced permeability in deeper gassy coal seam," *Journal of China Coal Society*, vol. 39, no. 8, pp. 1650–1658, 2014.

[3] D. Wang, R. Lv, J. Wei, P. Zhang, C. Yu, and B. Yao, "An experimental study of the anisotropic permeability rule of coal containing gas," *Journal of Natural Gas Science and Engineering*, vol. 53, no. 5, pp. 67–73, 2018.

[4] L. Wang, Y.-P. Cheng, F.-R. Li, H.-F. Wang, and H.-B. Liu, "Fracture evolution and pressure relief gas drainage from distant protected coal seams under an extremely thick key stratum," *Journal of China University of Mining and Technology*, vol. 18, no. 2, pp. 182–186, 2008.

[5] B. M. Shi and Z. G. Liu, "Numerical simulation of the upper coal and rock deformation characteristic caused by mining protecting stratum," *Journal of China Coal Society*, vol. 1, no. 4, pp. 595–599, 2010.

[6] W. Yang, B.-Q. Lin, Y.-A. Qu et al., "Stress evolution with time and space during mining of a coal seam," *International Journal of Rock Mechanics and Mining Sciences*, vol. 48, no. 7, pp. 1145–1152, 2011.

[7] Y. Zhao, L. Zhang, W. Wang, J. Tang, H. Lin, and W. Wan, "Transient pulse test and morphological analysis of single rock fractures," *International Journal of Rock Mechanics and Mining Sciences*, vol. 91, pp. 139–154, 2017.

[8] K. Jin, Y. Cheng, W. Wang, H. Liu, Z. Liu, and H. Zhang, "Evaluation of the remote lower protective seam mining for coal mine gas control: a typical case study from the Zhuxianzhuang coal mine, Huaibei Coalfield, China," *Journal of Natural Gas Science and Engineering*, vol. 33, pp. 44–55, 2016.

[9] H. T. Wang, Z.G. Wang, X.G. Fan, N.P. Liu, and J.C. Liu, "Numerical simulation for protection scope of steep inclined upper-protective layer of pitching oblique mining," *Disaster Advances*, vol. 3, no. 4, pp. 546–550, 2010.

[10] W. Yin, X. Miao, J. Zhang, and S. Zhong, "Mechanical analysis of effective pressure relief protection range of upper protective seam mining," *International Journal of Mining Science and Technology*, vol. 27, no. 3, pp. 537–543, 2017.

[11] S. G. Li, L. Suo, and H. F. Lin, "Numerical simulation of pressure relief effects of protective layer mining in different distances," *Journal of Liaoning Technical University*, vol. 33, no. 3, pp. 294–297, 2014.

[12] W. Yang, "Mechanical behavior evolution of mining stope and gas control technology," Ph.D. thesis, China University of Mining and Technology, Xuzhou, China, 2013.

[13] W. J. Lei, G. H. Wang, and X. X. Xue, "Application of finite element strength reduction method to destruction in coal seam floor," *Rock and Soil Mechanics*, vol. 32, no. 1, pp. 299–303, 2011.

[14] H. F. Wang, "Pressure relief functional principal of stope underlying coal-rock mass and application in gas extraction of protected coal seam," Ph.D. thesis, China University of Mining and Technology, Xuzhou, China, 2008.

[15] H. Y. Liu, Y. P. Cheng, C. C. Zhao et al., "Classification and judgment method of the protective layers," *Journal of Mining & Safety Engineering*, vol. 27, no. 4, pp. 468–474, 2010.

[16] National Coal Mine Safety Supervision Bureau, *Provisions of the Prevention of Coal and Gas Outburst*, China Coal Industry Publishing House, Beijing, China, 2009.

[17] Z. G. Yuan, H. T. Wang, X. H. Li et al., "Numerical simulation for protection scope of upper protective seam in steeply inclined multi-coal seam," *Journal of China Coal Society*, vol. 34, no. 5, pp. 594–598, 2009.

[18] Y. Zhao, Y. Wang, W. Wang, W. Wan, and J. Tang, "Modeling of non-linear rheological behavior of hard rock using triaxial rheological experiment," *International Journal of Rock Mechanics and Mining Sciences*, vol. 93, pp. 66–75, 2017.

[19] D. O. Potyondy and P. A. Cundall, "A bonded-particle model for rock," *International Journal of Rock Mechanics and Mining Sciences*, vol. 41, no. 8, pp. 1329–1364, 2004.

[20] L. Li, M. Y. Wang, P. X. Fan, H. Jiang, Y. Cheng, and D. Wang, "Strain rockbursts simulated by low-strength brittle equivalent materials," *Advances in Materials Science and Engineering*, vol. 2016, Article ID 5341904, 11 pages, 2016.

[21] C. Mei, Q. Fang, H. W. Luo, J. Yin, and X. Fu, "A synthetic material to simulate soft rocks and its applications for model studies of socketed piles," *Advances in Materials Science and Engineering*, vol. 2017, Article ID 1565438, 8 pages, 2017.

[22] S. Chen, H. Wang, J. Zhang, H. Xing, and H. Wang, "Experimental study on low-strength similar-material proportioning and properties for coal mining," *Advances in Materials Science and Engineering*, vol. 2015, Article ID 696501, 6 pages, 2015.

[23] X. Chen, Y. Wang, Y. Mei, and X. Zhang, "Numerical simulation on zonal disintegration in deep surrounding rock mass," *The Scientific World Journal*, vol. 2014, Article ID 379326, 8 pages, 2014.

[24] H. Kong, L. Wang, G. Q. Gu, and B. Xu, "Application of DICM on similar material simulation experiment for rock-like materials," *Advances in Civil Engineering*, vol. 2018, Article ID 5634109, 15 pages, 2018.

[25] Z. Yuan and Y. Shao, "Numerical modeling on hydraulic fracturing in coal-rock mass for enhancing gas drainage," *Advances in Civil Engineering*, vol. 2018, Article ID 1485672, 16 pages, 2018.

[26] Y. Zhao, L. Zhang, W. Wang, C. Pu, W. Wan, and J. Tang, "Cracking and stress-strain behavior of rock-like material containing two flaws under uniaxial compression," *Rock Mechanics and Rock Engineering*, vol. 49, no. 7, pp. 2665–2687, 2016.

[27] M. Karakus and B. Tutmez, "Fuzzy and multiple regression modelling for evaluation of intact rock strength based on point load, schmidt hammer and sonic velocity," *Rock Mechanics and Rock Engineering*, vol. 39, no. 1, pp. 45–57, 2005.

[28] H. Liu and Y. Cheng, "The elimination of coal and gas outburst disasters by long distance lower protective seam mining combined with stress-relief gas extraction in the Huaibei coal mine area," *Journal of Natural Gas Science and Engineering*, vol. 27, no. 1, pp. 346–353, 2015.

[29] Q. X. Yu and Y. P. Cheng, *Coal Mine Gas Control*, China University of Mining and Technology Press, Xuzhou, China, 2012.

[30] Y. L. Zhao, L. Y. Zhang, W. J. Wang et al., "Separation of elasto-visco-plastic strains of rock and a nonlinear creep model," *International Journal of Geomechanics*, vol. 18, no. 1, article 04017129, 2018.

[31] Y. Zhao, L. Zhang, W. Wang et al., "Creep behavior of intact and cracked limestone under multi-level loading and unloading cycles," *Rock Mechanics and Rock Engineering*, vol. 50, no. 6, pp. 1409–1424, 2017.